CORA Cork Open Research Archive
Cartlann Taighde Oscailte Chorcaí

Title	Analysis of electron mobility in HfO2/TiN gate metal-oxide-semiconductor field effect transistors: The influence of HfO2 thickness, temperature, and oxide charge
Author(s)	Negara, Muhammad A.; Cherkaoui, Karim; Hurley, Paul K.; Young, C. D.; Majhi, P.; Tsai, W.; Bauza, D.; Ghibaudo, G.
Publication date	2009-01-27
Original citation	Negara, M. A., Cherkaoui, K., Hurley, P. K., Young, C. D., Majhi, P., Tsai, W., Bauza, D. and Ghibaudo, G. (2009) 'Analysis of electron mobility in HfO2/TiN gate metal-oxide-semiconductor field effect transistors: The influence of HfO2 thickness, temperature, and oxide charge', Journal of Applied Physics, 105(2), pp. 024510. doi: 10.1063/1.3068367
Type of publication	Article (peer-reviewed)
Link to publisher's version	http://aip.scitation.org/doi/abs/10.1063/1.3068367 http://dx.doi.org/10.1063/1.3068367 Access to the full text of the published version may require a subscription.
Rights	**© 2009 American Institute of Physics, This article may be downloaded for personal use only. Any other use requires prior permission of the author and AIP Publishing. The following article appeared in Negara, M. A., Cherkaoui, K., Hurley, P. K., Young, C. D., Majhi, P., Tsai, W., Bauza, D. and Ghibaudo, G. (2009) 'Analysis of electron mobility in HfO2/TiN gate metal-oxide-semiconductor field effect transistors: The influence of HfO2 thickness, temperature, and oxide charge', Journal of Applied Physics, 105(2), pp. 024510. doi: 10.1063/1.3068367 and may be found at http://aip.scitation.org/doi/abs/10.1063/1.3068367**
Item downloaded from	http://hdl.handle.net/10468/4217

Downloaded on 2018-08-23T18:39:46Z

UCC
University College Cork, Ireland
Coláiste na hOllscoile Corcaigh

Analysis of electron mobility in HfO_2/TiN gate metal-oxide-semiconductor field effect transistors: The influence of HfO_2 thickness, temperature, and oxide charge

M. A. Negara' , K. Cherkaoui, P. K. Hurley, C. D. Young, P. Majhi, W. Tsai, D. Bauza, and G. Ghibaudo

Citation: Journal of Applied Physics **105**, 024510 (2009); doi: 10.1063/1.3068367
View online: http://dx.doi.org/10.1063/1.3068367
View Table of Contents: http://aip.scitation.org/toc/jap/105/2
Published by the American Institute of Physics

Analysis of electron mobility in HfO_2/TiN gate metal-oxide-semiconductor field effect transistors: The influence of HfO_2 thickness, temperature, and oxide charge

M. A. Negara,[1,a)] K. Cherkaoui,[1] P. K. Hurley,[1] C. D. Young,[2] P. Majhi,[3] W. Tsai,[3] D. Bauza,[4] and G. Ghibaudo[4]
[1]*Tyndall National Institute, University College Cork, Cork, Ireland*
[2]*SEMATECH, 2706 Montopolis Drive, Austin, Texas 78741, USA*
[3]*Intel Corporation, SC1-05, 2200 Mission College Boulevard, Santa Clara, California 95054-1549, USA*
[4]*IMEP, ENSERG, BP 257, 38016 Grenoble, France*

(Received 10 September 2008; accepted 8 December 2008; published online 27 January 2009)

We report a new analysis of electron mobility in HfO_2/TiN gate metal-oxide-semiconductor field effect transistors (MOSFETs) by investigating the influence of HfO_2 thickness (1.6–3 nm), temperature (50–350 K), and oxide charge ($\sim 1\times10^{11}-8\times10^{12}$ cm^{-2}) in the high inversion charge region. The fixed oxide charge and interface state densities are deliberately increased using negative-bias-temperature stress, allowing the determination of the Coulomb scattering term as a function of temperature for various oxide charge levels. The temperature dependence of the Coulomb scattering term is consistent with the case of a strongly screened Coulomb potential. Using the experimentally determined temperature dependence of Coulomb scattering term, a model is developed for the electron mobility, including the effects oxide charge (μ_C), high-k phonon ($\mu_{Ph\text{-}Hk}$), silicon phonon ($\mu_{Ph\text{-}Si}$), and surface roughness scattering (μ_{SR}). The model provides an accurate description of the experimental data for variations in HfO_2 thickness, temperature, and oxide charge. Using the model the relative contributions of each mobility component are presented for varying oxide charge and high-k thickness. Scaling of the HfO_2 physical thickness provided a reduction in the oxide charge and high-k phonon scattering mechanisms, leading to an increase in electron mobility in HfO_2/TiN gate MOSFETs. © *2009 American Institute of Physics*.
[DOI: 10.1063/1.3068367]

I. INTRODUCTION

The scaling of silicon based metal-oxide-semiconductor field effect transistors (MOSFETs) is approaching physical limits imposed by the atomic structure. The continuing miniaturization of complementary MOSFET technologies introduces new challenges relating to power, heat, and particle behavior. To overcome the power dissipation and heating problem arising from the gate leakage, high-dielectric constant (high-k) materials have been proposed. Replacing conventional SiO_2 with high-k materials for the gate insulator allows the same equivalent oxide thickness (E_{OT}) to be obtained for a physically thicker gate oxide, leading to significant gate oxide leakage suppression.

Hafnium-based high-k dielectrics and metal gate electrodes have been extensively investigated as alternative gate materials,[1–11] and the successful incorporation of hafnium based high-k materials into the gate stack of MOSFETs with minimum feature sizes of 45 nm has recently been announced.[12] However, there are still many issues associated with the implementation of these materials. One crucial problem for the hafnium-based high-k dielectrics technology integration is the quality of the dielectric-silicon system with regard to its electrical and structural properties, especially in terms of high-k phonon interaction, oxide charges, and their influence on electron and hole mobility.

A degradation of electron mobility is commonly reported for HfO_2/TiN gate MOSFETs.[1–11] This degradation has been attributed to the contributions of oxide charge in the high-k layer (columbic scattering), high-k phonon scattering, silicon phonon scattering, and surface roughness scattering. It has recently been demonstrated that interface defect densities in the range of $(3-4)\times10^{10}$ cm^{-2} and fixed positive oxide charge densities $<2\times10^{12}$ cm^{-2} do not yield significant mobility degradation.[1,9] The increased Coulomb scattering alone cannot account for all of the mobility degradation observed in HfO_2/TiN gate n-MOSFETs. An additional scattering mechanism due to soft optical phonons in the high-k layer has been theoretically predicted by Fischetti *et al.*,[10] and experimental evidence of the soft optical phonons influence on carriers mobility was found through temperature dependence studies.[2–10] The beneficial effect of metal gate electrode screening on the high-k phonon-electron interaction has been reported by Datta *et al.*[2] and Chau *et al.*[3] to result in a higher mobility value than measured in the corresponding high-k/polysilicon gate stacks. However, a more recent work by Maitra *et al.*[8] did not observe a difference between polysilicon or metal gate electrodes for HfO_2 gate MOSFETs. We do not consider the issue of metal gate screening in this study. All of the MOSFETs examined have TiN gate electrodes.

Most of the published works to date were carried out on one or two high-k thickness values and with several interface

a)Electronic mail: adi.negara@tyndall.ie.

 © 2009 American Institute of Physics

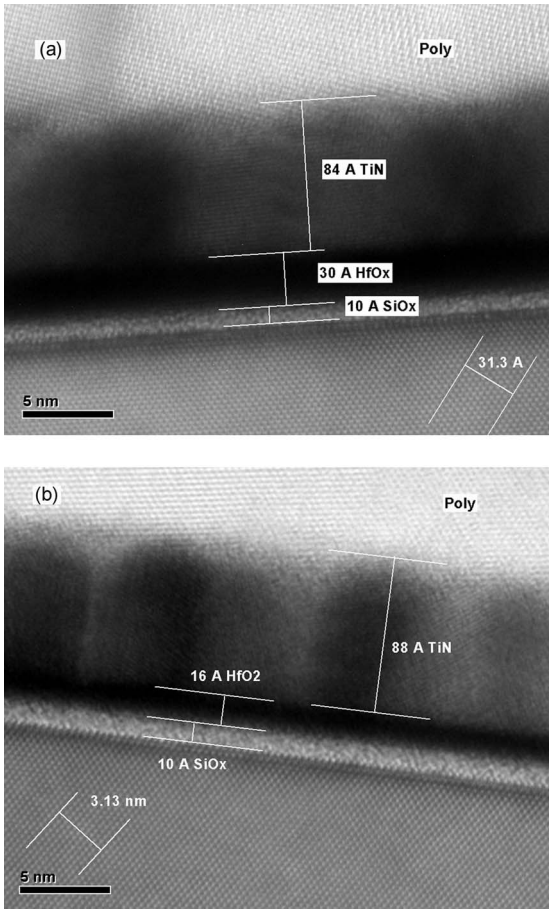

FIG. 1. High resolution TEM images through the gate stack region for (a) 3 nm HfO_2/TiN gate *n*-MOSFET and (b) 1.6 nm HfO_2/TiN gate *n*-MOSFET.

oxide thicknesses, resulting in a linear temperature dependence of the Coulomb scattering especially at low inversion charge density.[2–9] In this paper, we report a detailed study of electron mobility at high inversion charge density ($\sim 8 \times 10^{12}$ cm^{-2}) in TiN/HfO_2/SiO_x/Si *n*-channel MOSFETs. The devices examined have HfO_2 film thickness values of 1.6, 2, 2.4, and 3 nm and a fixed interface SiO(N) layer of $\sim$1.0 nm with identical device processing in all respects, allowing us to examine the influence of HfO_2 thickness on mobility degradation.

We extend previous studies by using temperature bias stress to deliberately increase the density of interface states and fixed oxide charge.[9,11] The temperature dependence of the electron mobility from 50 to 350 K is determined before and after the various levels of oxide and interface degradations. This new approach provides an experimental route for the determination of the Coulomb scattering term as a function of temperature for various oxide charge levels. The silicon phonon and surface roughness contributions are modeled based on the analysis of Takagi *et al.*[13] This allows the determination of the high-*k* remote phonon scattering contribution over the temperature to be evaluated. The proposed model reproduces the experimental data as a function of temperature (50–350 K), HfO_2 thickness (1.6–3 nm) and total oxide charge ($\sim 1 \times 10^{11} - 8 \times 10^{12}$ cm^{-2}), allowing calculation of the percentage contribution of each mobility component.

TABLE I. Device details and extracted parameters. Van Dort analytical model and QM *C-V* curve fitting used for the determination of C_{ox}, E_{OT}, V_{FB}, and N_a.

Wafer	A	B	C	D
t-HfO_2 (nm)	1.6	2	2.4	3
t-SiO_x (nm)	1	1	1	1
$C_{ox\ eff}$ (F/cm^2)	2.43×10^{-6}	2.35×10^{-6}	2.25×10^{-6}	2.16×10^{-6}
V_{FB} (V)	−0.49	−0.51	−0.58	−0.6
$D_{it}+N_f$ (/cm^2)	1×10^{11}	4.7×10^{11}	9×10^{11}	1.54×10^{12}
E_{OT} (nm)	1.06	1.14	1.21	1.25
μ_{peak} (cm^2/V s)	225	212	195	178

II. EXPERIMENTAL DETAILS

In this study, we used 1.6, 2, 2.4, and 3 nm TiN/HfO_2 gate MOSFETs, fabricated with atomic layer deposition (ALD), with $\sim$1 nm interface SiO_x layer. High resolution cross sectional transmission electron microscopy (TEM) images through the gate stack region of the 3 and 1.6 nm HfO_2/TiN gate *n*-MOSFETs are shown in Fig. 1. Isolated gate MOSFETs with 10×3 μm^2 areas have been used as test devices. The mobility was extracted from the split capacitance-voltage (*C-V*) technique at room temperature.[14] For low temperature measurements, the *Y* function method was used for mobility extraction.[15] The interface state density was calculated from the maximum charge pumping current after the leakage current correction.[16,17] The negative bias temperature stress (NBTI) was performed at 180 °C. The stress duration was 20 min with mobility and charge pumping measurements evaluated subsequently at room temperature (25 °C). The oxide charges were calculated based on the flat band voltage shift of the measured *C-V* curves from the ideal values predicted by a quantum mechanical (QM) *C-V* simulator. The QM *C-V* simulator uses the modified Van Dort analytical model to account for QM effects.[14] The measurements were performed on wafer in a microchamber controlled environment (Cascade Microtech Summit 12971B) using an Agilent B1500. The low temperature measurements were carried out in a Suss MicroTec cryoprober.

III. RESULTS AND DISCUSSIONS

The device characteristics and electron mobility for the nondegraded devices have been reported previously.[9] Summary of the physical and electrical device parameters prior to degradation at 300 K is presented in Table I. The electron effective mobility as determined using the *Y* function and the split *C-V* approach is presented in Fig. 2. It is evident from Fig. 2 that for inversion charge densities of 8×10^{12} cm^{-2} and above, there is excellent agreement between the split *C-V* and *Y* function methods for all HfO_2 film thicknesses studied. As a consequence, the electron mobility extracted from the *Y* function method is focused on the condition of high inversion charge density ($\sim 8 \times 10^{12}$ cm^{-2}). It is noted that this is the condition relevant to logic device applications. A different method such as magnetoresistance will be needed to investigate the mobility at very low carrier density.[7]

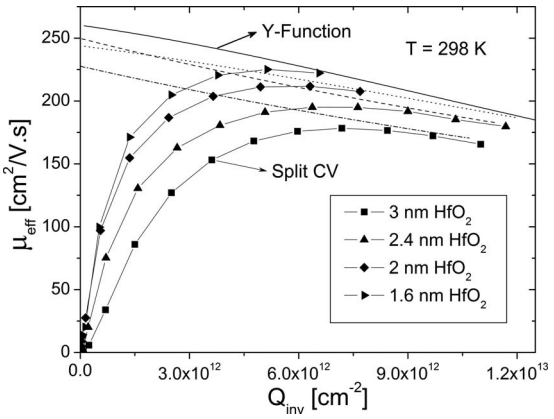

FIG. 2. Comparison between the electron mobility determined using the *Y* function and split *C-V* method at 298 K. Excellent agreement at high inversion charge (straight line=*Y* function).

Since we are working at a relatively high electric field region, the contributions of the silicon phonon and surface roughness scattering mechanisms to the overall electron mobility cannot be neglected. Following the approach used in a range of recent studies of mobility in high-k gate MOSFETs,[2–10] we use the Matthiessen's rule to provide an empirical model for the various contributions to the channel mobility by including soft optical phonon scattering in the high-k layer ($\mu_{\text{Ph-H}k}$), phonon scattering from the silicon channel region ($\mu_{\text{Ph-Si}}$), Coulomb scattering from bulk high-k and interface charge (μ_C), and surface roughness scattering (μ_{SR}).

$$\frac{1}{\mu} = \frac{1}{\mu_{\text{Ph-Si}}} + \frac{1}{\mu_{\text{SR}}} + \frac{1}{\mu_C} + \frac{1}{\mu_{\text{Ph-H}k}}. \tag{1}$$

The devices analyzed in this study exhibited no detectable fast transient charge trapping.[1,9]

From Table I, the initial positive oxide charge density scales with the HfO_2 thickness, with a maximum value of $\sim 1.5\times10^{12}$ cm^{-2} for the 3 nm HfO_2 film thickness MOSFET. To increase the density of fixed oxide charge and interface states, devices with the thickest HfO_2 film thickness of 3 nm (sample D) were subjected to NBTI.[18,19]

Figure 3(a) shows the evolution of the charge pumping characteristics with increasing stress bias. Experimentally it was determined that the interface state density (D_{it}) could be modified from the initial value of$\sim 4\times10^{10}-\sim 2\times10^{12}$ cm^{-2} with negative bias stress voltages from -1 to -2.7 V at 180 °C. Figure 3(b) shows the corresponding shift in the flat band voltage (V_{FB}).

The buildup of the fixed positive oxide charge and the interface state density as a function of the gate stress voltage are shown in Fig. 4. It is evident from this figure that the dominant contribution to the Coulomb scattering following NBTI is from the positive oxide charge. It is determined experimentally that for V_g stress >1.5 V that the ratio of N_f/D_{it} is ~ 5 for the n channel MOSFETs.

The Coulomb scattering parameter (α) can be determined from the relationship between interface state charges (D_{it}), oxide charge density (N_f), and the reciprocal mobility ($1/\mu$). We rewrite the reciprocal mobility model in Eq. (1)

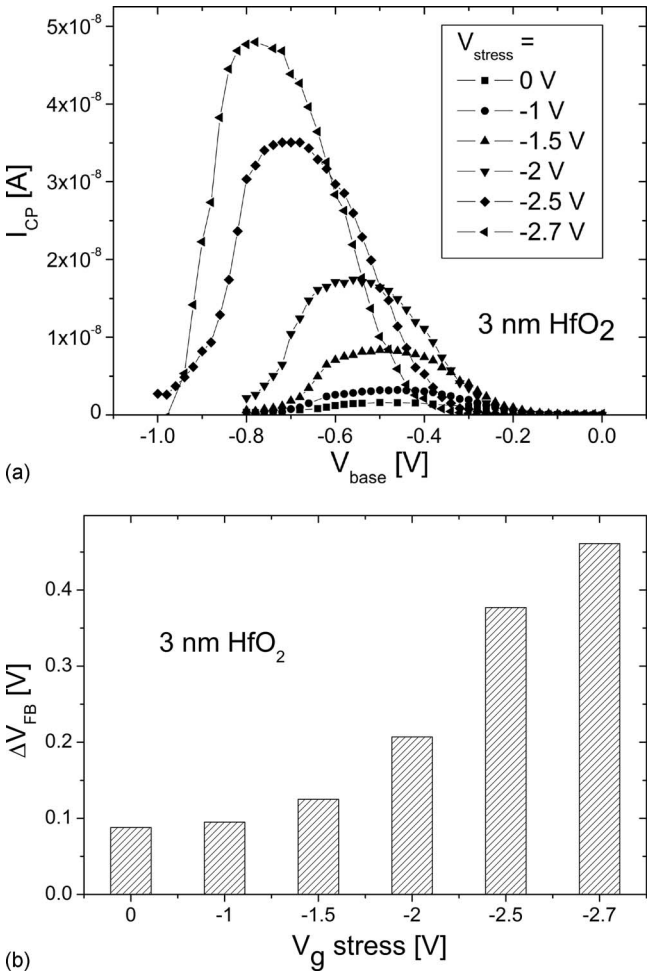

FIG. 3. (a) Charge pumping current of 3 nm HfO_2/TiN gate n-MOSFETs after gate leakage correction with the 1 MHz and 1 KHz ($W/L=10\ \mu$m/3 μm). For the charge pumping characteristics the pulse amplitude=+1 V, rise and fall times $t_r=t_f=50$ ns. (b) The corresponding ΔV_{FB} vs gate stress voltage.

into two separate components, i.e., one without the influence of charges and one with the influence of charges. Assuming at present that the scattering parameter (α) is independent of the temperature, the relationship can be described as follows:[20]

$$\frac{1}{\mu} = \frac{1}{\mu_{N_{\text{tot}}=0}} + \frac{1}{\mu_C} = \frac{1}{\mu_{N_{\text{tot}}=0}} + \alpha q(N_{\text{tot}}), \tag{2}$$

where $N_{\text{tot}}=D_{\text{it}}+N_f$ and $\mu_{N_{\text{tot}}=0}$ consists of the contributions from $\mu_{\text{Ph-H}k}$, $\mu_{\text{Ph-Si}}$, and μ_{SR}.

At room temperature, the effective mobility can be determined by using the split *C-V* method.[14] Figure 5 shows the reciprocal of the peak effective mobility of n-MOSFETs as function of N_f+D_{it} ($Q_{\text{inv}}\sim 6\times10^{12}$ cm^{-2}). We can see from Figs. 4 and 5 that the combined interface state and positive oxide charge do contribute to the mobility degradation following the NBTI. Moreover, the experimentally obtained linear relationship of the reciprocal peak mobility to the total charge observed in Fig. 6 is consistent with the model in Eq. (2).

From the reciprocal of the peak mobility versus N_{tot} in Fig. 5, we determine α to be 2565 V s/C for n channel

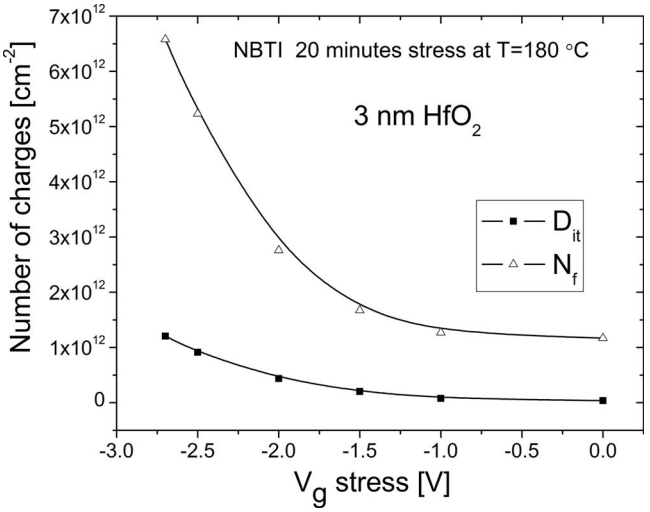

FIG. 4. The increase in fixed positive charge (N_f) and interface state density (D_{it}) as a function of gate bias during NBTI stressing for a 3 nm HfO_2 n-channel MOSFET ($W/L=10\ \mu m/3\ \mu m$).

MOSFETs at 298 K. It is a little bit lower than the value reported in Ref. 21, extracted from the $1/f$ noise measurement technique.

As the mobility in the case of zero oxide or interface charge ($\mu_{N_{tot}=0}$) is determined from the intercept in Fig. 5, we are now able to calculate the charges contribution to mobility degradation for the devices prior to negative bias stress. Prior to negative bias stress ($V_{stress}=0$), we determined $N_{tot}\sim 1.5\times 10^{12}/cm^2$ and $\mu_{eff}\sim 193\ cm^2/V\,s$. Hence, the initial charge density of $N_{tot}\sim 1.5\times 10^{12}/cm^2$ results in only a 7% degradation from the extrapolated zero charge mobility (from $\mu_{N_{tot}=0}=208\ cm^2/V\,s$). This relatively low level of degradation for $N_{tot}\sim 1.5\times 10^{12}/cm^2$ is in agreement with previous theoretical modeling,[22] predicting 5%–10% degradation of the mobility for $1-2\times 10^{12}/cm^2$ fixed oxide charges.

To gain further understanding of the relative contributions of the charge and phonon scattering terms to the overall electron mobility, measurements were performed on the 3 nm HfO_2 devices from 10 to 350 K using the Y function method to determine the mobility. These measurements were performed for both the nonstressed device and for devices following NBTI stressing to varying levels of oxide charge and interface state density.

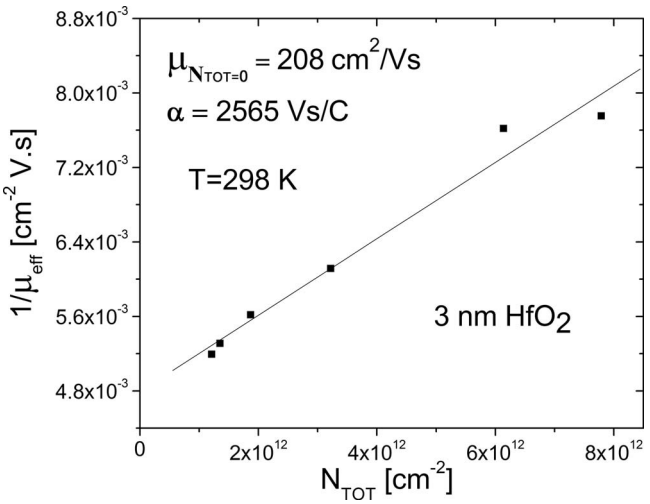

FIG. 5. Reciprocal of the peak effective mobility as a function of the total oxide charge ($N_{tot}=D_{it}+N_f$) for a 3 nm HfO_2 n-MOSFET ($W/L=10\ \mu m/3\ \mu m$). The slope of this characteristic yields the electron scattering parameter $\alpha\sim 2565$ V s/C. The intercept at $N_{tot}=0$ represents the mobility for the device without the influence of charges.

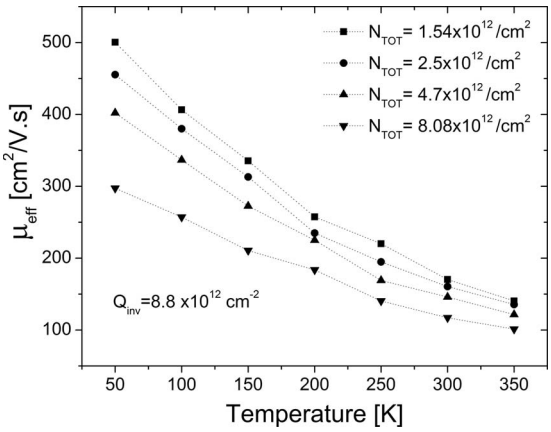

FIG. 6. Effective field electron mobility μ_{eff} at $Q_{inv}=8.8\times 10^{12}\ cm^{-2}$ for both nondegraded and degraded devices from 50 to 350 K for 3 nm HfO_2/TiN gate n-MOSFET ($W/L=10\ \mu m/3\ \mu m$). For fresh device, the total charge $N_{tot}=1.54\times 10^{12}/cm^2$.

The Y function method yields low field mobility from direct parameter extraction using $I_d(V_g)$ characteristics in strong inversion.[14,15] The corresponding effective mobility at a given surface inversion charge density can be determined using the first and second order mobility attenuation factors, as shown in Eq. (3),

$$\mu_{eff}=\frac{\mu_o}{1+\theta_1(V_g-V_t)+\theta_2(V_g-V_t)^2}, \tag{3}$$

where μ_o is the low field mobility, V_g is the gate voltage, V_t is the device threshold voltage, and θ_1 and θ_2 are the first and the second order mobility attenuation factors extracted from the Y function method. We extracted the effective mobility (μ_{eff}) at a relatively high inversion charge density ($Q_{inv}=8.8\times 10^{12}\ cm^{-2}$). As explained before, we selected the high Q_{inv} region since the mobility extracted from the Y-function is in excellent agreement with the split C-V method especially at high inversion charge (see Fig. 2). The resulting temperature dependent electron mobility (at $Q_{inv}\sim 8\times 10^{12}\ cm^{-2}$) is shown in Fig. 6 for four levels of total oxide charge from 1.54×10^{12} to $8.08\times 10^{12}\ cm^{-2}$. We can observe a significant mobility degradation for a stress induced total charge density of $N_{tot}=8.8\times 10^{12}\ cm^{-2}$.

In order to establish the influence of these charges on the mobility as a function of temperature, we plot the data $1/\mu_{eff}$ versus qN_{tot} for each temperature. As shown on Fig. 7, we found there is a change in gradient of the $1/\mu_{eff}$ versus qN_{tot} plot with the temperature, indicating the temperature dependence of the scattering parameter α. The relationship of α with temperature, as derived from the gradients in Fig. 7, is shown in Fig. 8.

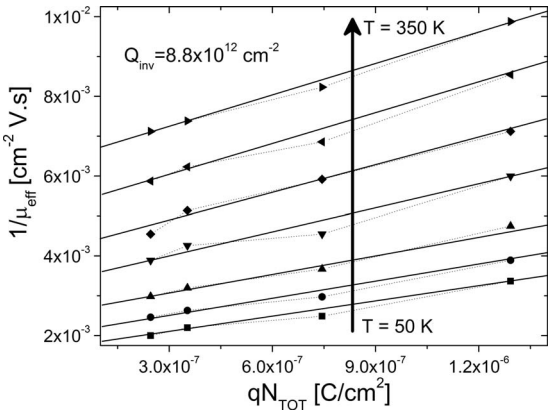

FIG. 7. Reciprocal of the effective mobility at $Q_{\text{inv}}=8.8\times10^{12}$ cm^{-2} as a function of the total charges ($D_{\text{it}}+N_f$) for n-MOSFETs for both stressed and fresh devices from 50 to 350 K with 50 K step, for 3 nm HfO_2/TiN gate n-MOSFET ($W/L=10$ μm/3 μm).

Based on the experimental results in Figs. 6–8, we can rewrite Eq. (2) to include a temperature dependence of the Coulomb scattering parameter as follows:

$$\frac{1}{\mu}=\frac{1}{\mu_{N_{\text{tot}}=0}}+\frac{1}{\mu_C}=\frac{1}{\mu_{N_{\text{tot}}=0}}+\alpha(T)q(N_{\text{tot}}). \tag{4}$$

From Fig. 8 the Coulomb scattering parameter increases with temperature with a nonlinear relationship. Over the temperature range of 50–250 K, α is approximately proportional to the square of the measurement temperature, as shown in the inset of Fig. 8. This behavior can be understood through a consideration of the temperature dependence of Coulomb scattering in the condition of an unscreened and a screened Coulomb potential. In the case of a relatively low inversion charge density, where screening of the high-k positive charge and interface charge by the inversion layer can be neglected, the Coulomb mobility, μ_C, takes the form[23]

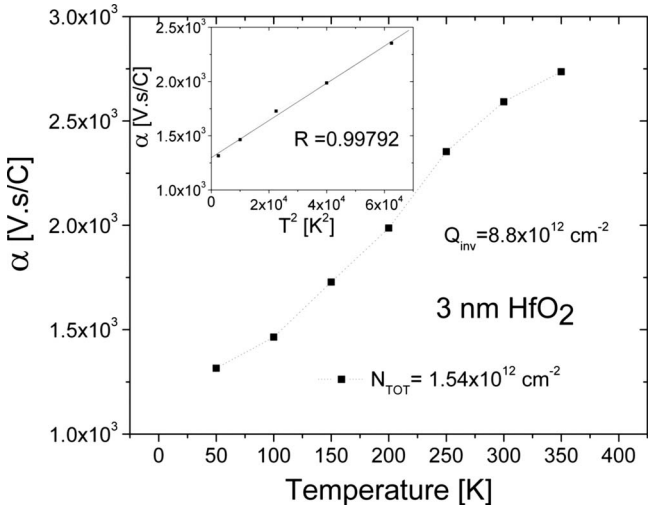

FIG. 8. Plot of α as a function of temperature for nondegraded and degraded n-MOSFETs from 50 to 350 K for 3 nm HfO_2/TiN gate n-MOSFET ($W/L=10$ μm/3 μm).

$$\mu_C=\frac{q}{m^*}\left(\frac{\bar{\varepsilon}}{q^2}\right)^2\frac{2\hbar k_B T}{\pi^2 N_{\text{tot}}}, \tag{5}$$

where $\bar{\varepsilon}=\frac{1}{2}(\varepsilon_{\text{Si}}+\varepsilon_{\text{ox}})$, m^* is the mobility effective mass, and N_{tot} is the average density of surface-oxide charges. From Eq. (5), in this nonscreened condition, $1/\mu_C$ is proportional to $1/T$. For a fresh device with N_{tot} value of 1.5×10^{12} cm^{-2} (sample D), Eq. (5) yields mobility values in the range from 10 to 50 cm^2/V s over the range from 50 to 300 K. The measured values over this range are from ~500 to 200 cm^2/V s, so the mobility values predicated by Eq. (5) are not consistent with the absolute mobility values or temperature dependence measured experimentally.

For the devices analyzed in this work the mobility was extracted in the condition of high inversion charge ($Q_{\text{inv}}\sim8\times10^{12}$ cm^{-2}). For this condition of high inversion charge, where screening of the Coulomb potential is very significant, the scattering rate due to the charges can be described as follows:[24]

$$\frac{1}{\tau_m(p)}=\frac{\pi N_{\text{tot}}}{\hbar}\left(\frac{q^2L_D^2}{\varepsilon_s\varepsilon_o}\right)^2 g_C(E), \tag{6}$$

where $L_D=\sqrt{\varepsilon_s\varepsilon_o k_B T/q^2 n_s}$ is known as the Debye length for nondegenerate condition and $g_C(E)$ is the density of state. E is the carrier energy that increases with temperature. τ_m is the momentum relaxation time. In this expression, $1/\tau_m$ represents the scattering rate.

Based on Eq. (6) and the relationship $\mu=q\tau_m(p)/m^*$, for the strongly screened condition, the temperature dependence of the reciprocal Coulomb mobility takes the form

$$\frac{1}{\mu_C}=\frac{g_C(E)(k_B T)^2\pi N_{\text{tot}}m^*}{q\hbar n_s^2}. \tag{7}$$

From Eq. (7), it is evident that in the screened condition, $1/\mu_C$, is proportional to T^2. From Eqs. (4) and (7), the empirical temperature dependent scattering parameter $\alpha(T)$, can be identified as

$$\alpha(T)=\frac{g_C(E)(k_B T)^2\pi m^*}{q^2\hbar n_s^2}. \tag{8}$$

The relationship of α to T^2 as predicted in Eq. (8) is measured over the temperature range from 50 to 250 K. The experimental results in Fig. 8 suggest that at higher temperatures additional factors influence $\alpha(T)$, leading to an attenuation of the change in α with temperature.

To simplify the modeling of the electron mobility we make a linear approximation to the temperature dependence of the Coulomb scattering parameter as follows:

$$\alpha(T)qN_{\text{tot}}=(mT+c). \tag{9}$$

By adding Eq. (9) into Eq. (1), we arrive at the following relationship for the mobility as a function of temperature:

$$\frac{1}{\mu}=\frac{1}{\mu_{\text{Ph-Si}}}+\frac{1}{\mu_{\text{SR}}}+\frac{1}{\mu_C}+\frac{1}{\mu_{\text{Ph-Hk}}}, \tag{10}$$

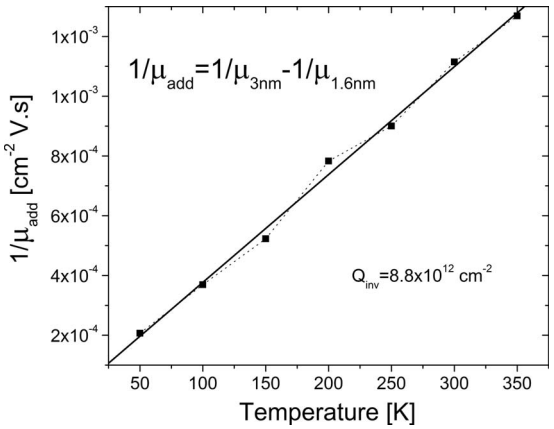

FIG. 9. The reciprocal mobility from an additional 1.4 nm HfO_2 thickness for TiN gate *n*-MOSFET ($W/L=10\ \mu m/3\ \mu m$).

$$\frac{1}{\mu}=\left[\frac{T^{1.75}}{\beta E_{\text{eff}}^{-0.3}}\right]+\left[\frac{1}{\gamma E_{\text{eff}}^{-2.6}}\right]+[mT+c]+[\lambda T]. \tag{11}$$

For $\mu_{\text{Ph-Si}}$ and μ_{SR} value, we used the expressions reported in Refs. 4 and 13 as follows:

$$\mu_{\text{Ph-Si}}=\beta E_{\text{eff}}^{-0.3}T^{-1.75},$$

where β is 2.0×10^5 mK/s for electrons,

$$\mu_{\text{SR}}=\gamma E_{\text{eff}}^{-2.6},$$

where γ is 4.5×10^{19} m/s.

We used this surface roughness model by assuming the high-*k* material has the same surface roughness as the SiO_2 system. The linear temperature dependence of the remote phonon scattering term $[\lambda T]$ used in Eq. (11) has been found experimentally in a range of publications.[3–5]

A justification for taking a linear dependence for α and phonon in high-*k* with temperature in Eq. (9) is presented in Fig. 9. By subtracting the mobility of MOSFETs with two different HfO_2 thicknesses (3 and 1.6 nm), only the $\mu_{\text{Ph-H}k}$ and μ_C components remain,

$$\frac{1}{\mu_{\text{add}}}=\frac{1}{\mu_{3\ \text{nm}}}-\frac{1}{\mu_{1.6\ \text{nm}}}=\frac{1}{\mu_C}+\frac{1}{\mu_{\text{Ph-H}k}}. \tag{12}$$

The reciprocal additional mobility in Fig. 9 does exhibit an approximately linear increase with the temperature, providing experimental justification for taking a linear temperature dependence of the Coulomb and remote phonon scattering terms in Eq. (11). Based on Figs. 2 and 9, it is evident that there is an influence of oxide thickness on the electron mobility for these high-*k* MOSFETs, since the remaining mobility terms originate either from Si or the SiO_x interlayer are similar for all samples.

As we characterized experimentally the Coulomb scattering contribution over temperature (50–350 K) and charge density ($1-8\times10^{12}$ cm^{-2}), the remote phonon scattering contribution from the high-*k* ($\mu_{\text{Ph-H}k}$) can be extracted by subtracting the total mobility μ_{eff} from the sum of the Coulomb, silicon phonon, and surface scattering terms. From the subtraction result, we found a linear dependence of $\mu_{\text{Ph-H}k}$ component λ with temperature. The parameters used to model the Coulomb scattering (*m* and *c*) and the remote phonon scattering (λ) contributions to the electron mobility over temperature, oxide charge, and HfO_2 film thickness are presented in Table II.

TABLE II. Parameters used in Eq. (11). *m* and *c* are the components of μ_C and λ is the $\mu_{\text{Ph-H}k}$ component.

t-HfO_2 (nm)	N_{tot} (cm^2)	*m* (V s/cm^2 K)	*c* (V s/cm^2)	λ (V s/cm^2 K)
1.6	1.0×10^{11}	7.8×10^{-8}	1.5×10^{-5}	9.0×10^{-7}
2	4.7×10^{11}	3.6×10^{-7}	7.2×10^{-5}	2.6×10^{-6}
2.4	9.0×10^{11}	7.0×10^{-7}	1.4×10^{-4}	2.7×10^{-6}
3	1.5×10^{12}	1.2×10^{-6}	2.4×10^{-4}	3.5×10^{-6}
3	2.5×10^{12}	1.9×10^{-6}	3.8×10^{-4}	3.5×10^{-6}
3	4.7×10^{12}	3.6×10^{-6}	7.2×10^{-4}	3.5×10^{-6}
3	8.0×10^{12}	6.3×10^{-6}	1.2×10^{-3}	3.5×10^{-6}

Figure 10 shows the modeling result for the 3 nm HfO_2 device over temperature (50–350 K) for total oxide charge densities of 1.54×10^{12}, 2.5×10^{12}, 4.7×10^{12}, and 8.08×10^{12} cm^{-2}. As we can see from the figure, the model provides an accurate description of the temperature and charge dependence of the mobility.

Figure 11 shows the mobility contributions for the various scattering terms for a nondegraded 3 nm HfO_2 device ($N_{\text{tot}}=1.54\times10^{12}$ cm^{-2}). We can see [Figs. 11(a) and 11(b)] that $1/\mu_C$ contributes only ~10% to the total mobility $1/\mu_{\text{eff}}$ at room temperature, in agreement with previous results in Fig. 5 and theoretical modeling in Ref. 22. As a result of the reduction in phonon vibration by lowering the temperature, the $1/\mu_C$ percentage contribution to $1/\mu_{\text{eff}}$ increases and reaches a maximum of ~15% at 50 K as shown in Fig. 11(b). Due to the high surface electric field, the $1/\mu_{\text{Ph-Si}}$ and $1/\mu_{\text{SR}}$ terms are significant contributors to the mobility for the entire temperature range. Comparing $1/\mu_{\text{Ph-H}k}$ and $1/\mu_C$, we can see that $1/\mu_{\text{Ph-H}k}$ is still dominant at high temperatures. At room temperature, the $1/\mu_{\text{Ph-H}k}$ term contributes ~20% to $1/\mu_{\text{eff}}$. The $1/\mu_C$ contribution is more significant below 100 K.

Figure 12 presents the corresponding mobility contributions for the 3 nm HfO_2 device following NBTI, with a total

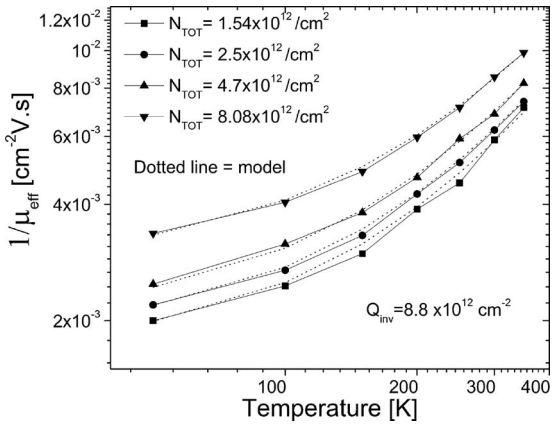

FIG. 10. Reciprocal μ_{eff} for both nondegraded and degraded devices from 50 to 350 K for 3 nm HfO_2/TiN gate *n*-MOSFET ($W/L=10\ \mu m/3\ \mu m$). For the nondegraded device, the total charge $N_{\text{tot}}=1.54\times10^{12}/cm^2$. The dot lines are the modeling μ_{eff} from Eq. (11).

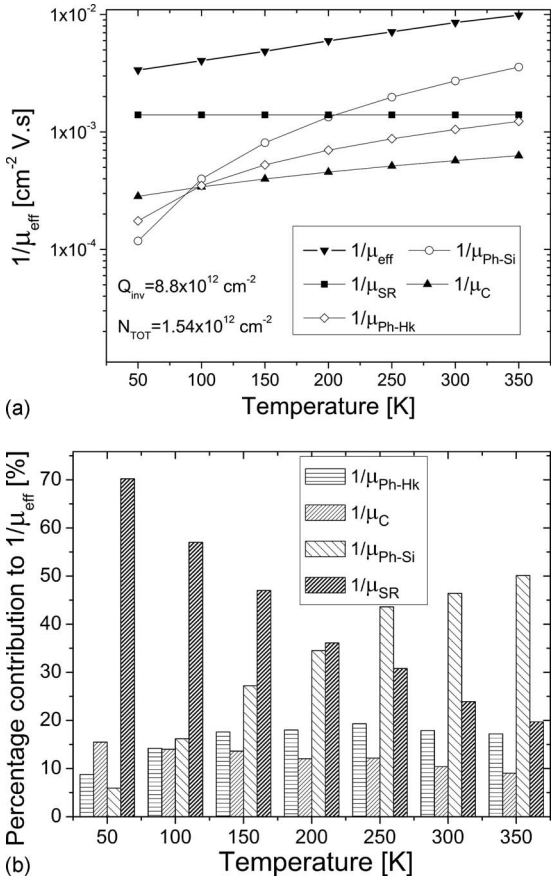

FIG. 11. (a) Calculated electron mobility components for $\mu_{\text{Ph-Si}}$, μ_{SR}, μ_C, and $\mu_{\text{Ph-}Hk}$ over the temperature range from 50 to 350 K for a nondegraded 3 nm HfO_2/TiN gate *n*-MOSFET ($W/L=10$ μm/3 μm). (b) The corresponding percentage contribution of the $1/\mu_C$, $1/\mu_{\text{Ph-Si}}$, $1/\mu_{\text{SR}}$, and $1/\mu_{\text{Ph-}Hk}$ to $1/\mu_{\text{eff}}$

oxide charge density of $N_{\text{tot}}=8.08\times10^{12}$ cm^{-2}. We can observe that $1/\mu_C$ is now the dominant contributor to $1/\mu_{\text{eff}}$ over the entire temperature range following the NBTI.

Since we know the total oxide charge for all the nondegraded samples (see Table I), we can now model the $1/\mu_C$ contribution for different HfO_2 thickness values over temperature. The $1/\mu_{\text{Ph-Si}}$ and $1/\mu_{\text{SR}}$ are assumed to remain unaltered for these samples. Only the remote phonon scattering

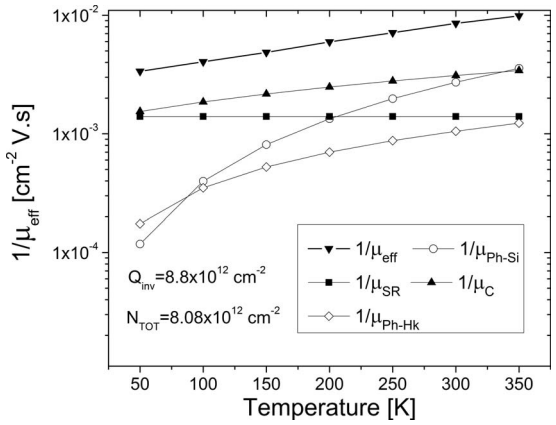

FIG. 12. Reciprocal μ_{eff}, $\mu_{\text{Ph-Si}}$, μ_{SR}, μ_C, and $\mu_{\text{Ph-}Hk}$ from 50 to 350 K for a degraded device 3 nm HfO_2/TiN gate *n*-MOSFET ($W/L=10$ μm/3 μm). $N_{\text{tot}}=8.08\times10^{12}$ cm^{-2}.

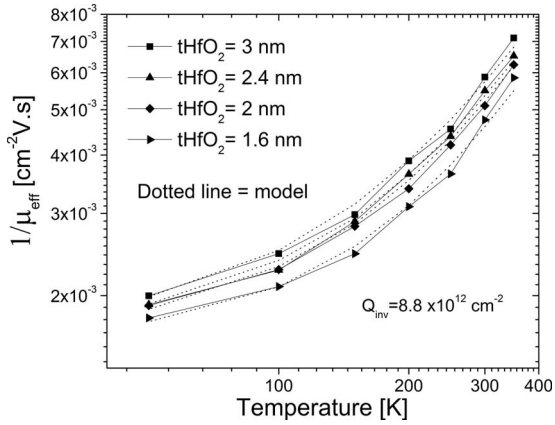

FIG. 13. Reciprocal μ_{eff} from 50 to 350 K for 3, 2.4, 2, and 1.6 nm HfO_2/TiN gate *n*-MOSFETs. The dot lines are the modeling μ_{eff} from Eq. (11).

term from the high-*k* layer ($1/\mu_{\text{Ph-}Hk}$) and the charge contributions in high-*k* layer ($1/\mu_C$) will vary with decreasing HfO_2 thickness. The $1/\mu_C$ contribution can be calculated from Eqs. (4) and (9) as the oxide charge and temperature dependence of α are known. The value of λ for all of the HfO_2 thicknesses can be determined by subtracting the total mobility $1/\mu_{\text{eff}}$ from the sum of the $1/\mu_C$, $1/\mu_{\text{Ph-}Hk}$, and $1/\mu_{\text{Ph-Si}}$ components. The modeling result is shown in Fig. 13 for the HfO_2 MOSFETs prior to degradation.

To compare the role of HfO_2 thickness, we plot the mobility components for thinnest HfO_2 thickness of 1.6 nm (sample A) in Fig. 14. From Fig. 15, we can see that by decreasing the HfO_2 thickness, the $1/\mu_C$ contribution becomes negligible. In addition, from Table II the remote phonon scattering (λ) parameter and the Coulomb scattering (*m* and *c*) parameters both exhibit increased values with increasing HfO_2 film thickness.

IV. CONCLUSIONS

The influences of HfO_2 thickness, temperature, and oxide charge on electron mobility have been investigated for ALD HfO_2/TiN gate *n*-MOSFETs for the condition of high inversion charge. We extended previous studies by using temperature bias stress to deliberately increase the density of interface states and fixed oxide charge, allowing the Coulomb scattering term as a function of temperature (50–350 K) to be determined for various oxide charge levels. The experimentally determined Coulomb scattering term was incorporated into a model for electron mobility including the effects oxide charge (μ_C), high-*k* phonon ($\mu_{\text{Ph-}Hk}$), silicon phonon ($\mu_{\text{Ph-Si}}$), and surface roughness scattering (μ_{SR}). The model provides an accurate description of the electron mobility for variations in HfO_2 thickness (1.6–3 nm), temperature (50–350 K), and oxide charge ($\sim1\times10^{11}$–8×10^{12} cm^{-2}).

For a 3 nm HfO_2 device, with a total charge density of $\sim2\times10^{12}$ cm^{-2} at room temperature, we find relative contributions to the electron mobility of 10% ($1/\mu_C$), 20% ($1/\mu_{\text{Ph-}Hk}$), 46% ($1/\mu_{\text{Ph-Si}}$), and 24% ($1/\mu_{\text{SR}}$). By reducing the physical thickness of the HfO_2 to 1.6 nm, the $1/\mu_C$ contribution becomes negligible, with relative contributions of

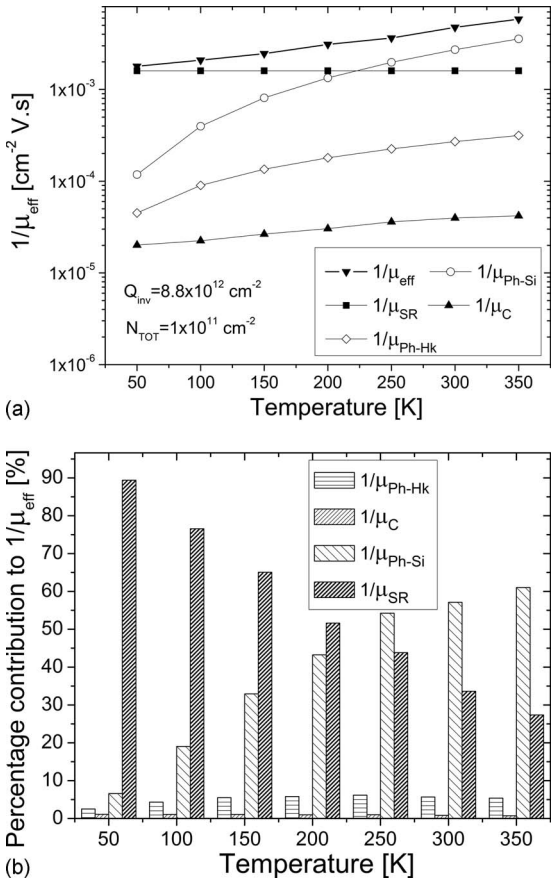

FIG. 14. (a) Reciprocal μ_{eff}, $\mu_{\text{Ph-Si}}$, μ_{SR}, μ_C, and $\mu_{\text{Ph-}Hk}$ from 50 to 350 K for fresh device 1.6 nm HfO_2/TiN gate *n*-MOSFET (W/L =10 μm/3 μm). (b) The corresponding percentage contribution of the $1/\mu_C$, $1/\mu_{\text{Ph-Si}}$, $1/\mu_{\text{SR}}$, and $\mu_{\text{Ph-}Hk}$ to $1/\mu_{\text{eff}}$

1% ($1/\mu_C$), 7% ($1/\mu_{\text{Ph-}Hk}$), 58% ($1/\mu_{\text{Ph-Si}}$), and 34% ($1/\mu_{\text{SR}}$). For the HfO_2 samples examined in this study, scaling of the HfO_2 physical thickness provided a reduction in the oxide charge and high-*k* phonon scattering mechanisms, leading to an increase in electron mobility in HfO_2/TiN gate MOSFETs.

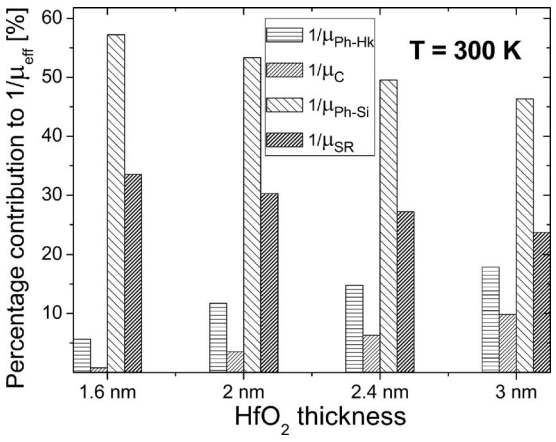

FIG. 15. The corresponding percentage contribution of the $1/\mu_C$, $1/\mu_{\text{Ph-Si}}$, $1/\mu_{\text{SR}}$, and $\mu_{\text{Ph-}Hk}$ to $1/\mu_{\text{eff}}$ for 1.6, 2, 2.4, and 3 nm HfO_2/TiN gate *n*-MOSFET (W/L=10 μm/3 μm) at T=300 K.

ACKNOWLEDGMENTS

The authors would like to thank Intel and SEMATECH for providing the TiN/HfO_2 transistor samples. The courtesy of R. Dunne, S. Cosgrove, and M. Brennan (Intel Ireland), who performed the TEM analysis, is gratefully acknowledged. Special thanks is due to Xavier Mescot for his assistance during the measurements at IMEP. This work was supported by Intel Ireland, the European Commission under the frame of the Network of Excellence "SINANO" and the Science Foundation Ireland (Grant No. 05/IN/1751).

[1] J. H. Sim, S. C. Song, P. D. Kirsch, C. D. Young, R. Choi, D. L. Kwong, B. H. Lee, and G. Bersuker, Microelectron. Eng. **80**, 218 (2005).
[2] S. Datta, G. Dewey, M. Doczy, B. S. Doyle, B. Jin, J. Kavalieros, R. Kotlyar, M. Metz, N. Zelickand, and R. Chau, Tech. Dig. - Int. Electron Devices Meet. **2003**, 28.1.1.
[3] R. Chau, S. Datta, M. Doczy, B. Doyle, J. Kavalieros, and M. Metz, IEEE Electron Device Lett. **25**, 408 (2004).
[4] W. J. Zhu and T. P. Ma, IEEE Electron Device Lett. **25**, 89 (2004).
[5] O. Weber, M. Casse, L. Thevenod, F. Ducroquet, T. Ernst, B. Guillaumot, and S. Deleonibus, Proceedings of the ESSDERC 2006, 2005 (unpublished), p. 379.
[6] Z. Ren, M. Fischetti, E. P. Gusev, E. Cartier, and M. Chudzik, Tech. Dig. - Int. Electron Devices Meet. **2003**, 793.
[7] L. Thevenod, M. Cassé, W. Desrat, M. Mouis, G. Reimbold, and F. Boulanger, Appl. Phys. Lett. **90**, 152111 (2007).
[8] K. Maitra, M. M. Frank, V. Narayanan, V. Misra, and E. A. Cartier, J. Appl. Phys. **102**, 114507 (2007).
[9] M. A. Negara, K. Cherkaoui, P. Majhi, C. D. Young, W. Tsai, D. Bauza, G. Ghibaudo, and P. K. Hurley, Microelectron. Eng. **84**, 1874 (2007).
[10] M. V. Fischetti, D. A. Neumayer, and E. A. Cartier, J. Appl. Phys. **90**, 4587 (2001).
[11] F. Lime, K. Oshima, M. Casse, G. Ghibaudo, S. Cristoloveanu, B. Guillaumot, and H. Iwai, Solid-State Electron. **47**, 1617 (2003).
[12] K. Mistry, C. Allen, C. Auth, B. Beattie, D. Bergstrom, M. Bost, M. Brazier, M. Buehler, A. Cappellani, R. Chau, C.-H. Choi, G. Ding, K. Fischer, T. Ghani, R. Grover, W. Han, D. Hanken, M. Hattendorf, J. He, J. Hicks, R. Huessner, D. Ingerly, P. Jain, R. James, L. Jong, S. Joshi, C. Kenyon, K. Kuhn, K. Lee, H. Liu, J. Maiz, B. McIntyre, P. Moon, J. Neirynck, S. Pae, C. Parker, D. Parsons, C. Prasad, L. Pipes, M. Prince, P. Ranade, T. Reynolds, J. Sandford, L. Shifren, J. Sebastian, J. Seiple, D. Simon, S. Sivakumar, P. Smith, C. Thomas, T. Troeger, P. Vandervoorn, S. Williams, and K. Zawadzki, Tech. Dig. - Int. Electron Devices Meet. **2007**, 247.
[13] S. Takagi, A. Toriumi, M. Iwase, and H. Tango, IEEE Trans. Electron Devices **41**, 2357 (1994).
[14] F. Lime, C. Guiducci, R. Clerc, G. Ghibaudo, C. Leroux, and T. Ernst, Solid-State Electron. **47**, 1147 (2003).
[15] G. Ghibaudo, Electron. Lett. **24**, 543 (1988).
[16] D. Bauza, IEEE Electron Device Lett. **23**, 658 (2002).
[17] P. Masson, J. L. Autran, and J. Brini, IEEE Electron Device Lett. **20**, 92 (1999).
[18] S. Zafar, B. H. Lee, and J. Stathis, IEEE Electron Device Lett. **25**, 153 (2004).
[19] M. Houssa, S. De Gendt, J. L. Autran, G. Groeseneken, and M. M. Heyns, Appl. Phys. Lett. **85**, 2101 (2004).
[20] G. Ghibaudo, O. Roux, Ch. Nguyen-Duc, F. Balestra, and J. Brini, Phys. Status Solidi A **124**, 571 (1991).
[21] C. Claeys, E. Simoen, A. Mercha, L. Pantisano, and E. Young, J. Electrochem. Soc. **152**, F115 (2005).
[22] M. Ono, T. Ishihara, and A. Nishiyama, IEEE Trans. Electron Devices **51**, 732 (2004).
[23] C. T. Sah, T. H. Ning, and L. L. Tschoopp, Surf. Sci. **32**, 561 (1972).
[24] M. Lundstrom, *Fundamentals of Carrier Transport* (Cambridge University Press, New York, 2000).